

Experimental study of tune-out wavelengths for spin-dependent optical lattice in ^{87}Rb Bose–Einstein condensation

KAI WEN,^{1,2}  ZENGMING MENG,^{1,2,*} LIANGWEI WANG,^{1,2} LIANGCHAO CHEN,^{1,2}
LIANGHUI HUANG,^{1,2} PENGJUN WANG,^{1,2} AND JING ZHANG^{1,2,3}

¹State Key Laboratory of Quantum Optics and Quantum Optics Devices, Institute of Opto-Electronics, Shanxi University, Taiyuan, Shanxi 030006, China

²Collaborative Innovation Center of Extreme Optics, Shanxi University, Taiyuan, Shanxi 030006, China

³e-mail: jzhang74@yahoo.com

*Corresponding author: zmmeng01@sxu.edu.cn

Received 27 May 2021; revised 1 August 2021; accepted 24 August 2021; posted 27 August 2021 (Doc. ID 432448); published 6 October 2021

We study the periodic potential of a one-dimensional optical lattice originating from a scalar shift and vector shift by manipulating the lattice polarizations. The ac Stark shift of an optical lattice is measured by Kapitza–Dirac scattering of ^{87}Rb Bose–Einstein condensate, and the characteristics of a spin-dependent optical lattice are presented by scanning the lattice wavelength between the D1 and D2 lines. At the same time, tune-out wavelengths that the ac Stark shift cancels can be probed by the optical lattice. We give the tune-out wavelengths in more general cases of balancing the contributions of both scalar and vector shifts. Our results provide a clear interpretation for a spin-dependent optical lattice and tune-out wavelengths, and help to design it by choosing the appropriate lattice wavelength. © 2021 Optical Society of America

<https://doi.org/10.1364/JOSAB.432448>

1. INTRODUCTION

The optical lattice for ultracold atoms has become an increasingly important technology in many-body physics [1], quantum simulation, quantum computation, quantum information storage, and high precision measurements [2–6]. When neutral atoms are trapped in periodic potentials produced by standing waves of light fields, the trapping potentials of various atomic internal states are manipulated by lattice polarizations, which is called the spin-dependent optical lattice [7,8], which brings more complicated geometry to ultracold atoms such as a spin-dependent hexagonal lattice [9] and spin-dependent optical superlattice [10], and has been used to study many interesting phenomena such as controlled coherent transport [7,11], spinor Bose–Einstein condensate (BEC) [12], spin–orbit coupling and artificial gauge fields [13,14], spontaneous emission of matter waves [15], and twisted-bilayer optical potentials [16].

Tune-out wavelengths that ac the Stark shift cancels were initially introduced in species-specific optical manipulation [17] and can be useful for optical Feshbach resonances [18] and atomic interferometers [19]. Since tune-out wavelengths are independent of light intensity [20–22], they can be precisely measured by various methods [23–30]. In general, a tune-out wavelength is utilized accurately only for the scalar shift by

canceling and neglecting the vector and tensor contributions as much as possible [23–25,28]. In this paper, we investigate tune-out wavelengths in more general cases of considering the contributions from both scalar and vector shifts. The ac Stark shift of an optical lattice is measured by Kapitza–Dirac scattering, which diffracts BEC into a number of high momentum states, and the characteristics of spin-dependent optical lattices are investigated by scanning the lattice wavelength between the D1 and D2 lines. Kapitza–Dirac scattering is a standard tool and shows many applications in calibrating the lattice depth [31–35], detecting the lattice structure [36,37], and performing high-resolution spectroscopy [38] and metrology [39,40]. The periodic potential originated from scalar and vector shifts is manipulated by controlling lattice polarizations, which is used to generate a spin-dependent optical lattice. We can design the special spin-dependent optical lattice with the help of tune-out wavelengths.

2. THEORY

A. ac Stark Shift

As we know, the ac Stark effect is the result of an interaction between atoms and a classical light field. Here, the total ac Stark

shift for alkali–metal atoms in the ground state interacting with a far-off-resonance light field can be expressed in terms of its scalar, vector, and tensor components [41–45]:

$$\begin{aligned} \Delta U &= \Delta U(F, m_F; \omega) \\ &= -A \left[\alpha^{(0)}(\omega) + \alpha^{(1)}(\omega) (\xi \hat{e}_k \cdot \hat{e}_B) \frac{m_F}{F} \right. \\ &\quad \left. + \alpha^{(2)}(\omega) \frac{3 \cos^2 \theta - 1}{2} \frac{3m_F^2 - F(F+1)}{F(2F-1)} \right], \quad (1) \end{aligned}$$

where $\alpha^{(0,1,2)}(\omega)$ are the scalar, vector, and tensor polarizabilities respectively. F is the total atomic angular momentum, m_F is the magnetic quantum number, A , is laser field intensity with $A = 2\epsilon_0 c |E|^2$, ω and E are the frequency and amplitude of the optical field, respectively, $\hat{e}_k \cdot \hat{e}_B = |e_k||e_B| \cos(\phi)$, \hat{e}_k and \hat{e}_B are unit vectors along the light wave vector and magnetic field quantization axis, respectively, ϕ is the intersection angle between \hat{e}_k and \hat{e}_B , θ is the intersection angle between the linearly polarized component of the light field and \hat{e}_B . This formula comes from the first non-vanishing term (second order) of a perturbation development. Note that the range of values of light ellipticity is $\xi \in [-1, 1]$, and $\xi = \pm 1$ denotes left and right circular polarizations. Left and right elliptical polarizations are defined in terms of the light wave vector. The scalar shift can be interpreted as a spin-independent light shift. The vector shift acts like an effective magnetic field to generate linear Zeeman splitting (light shift proportional to m_F), which depends on the ellipticity of light and the intersection angle between the laser beam wave vector and magnetic field quantization axis \hat{e}_B . The tensor shift is proportional to m_F^2 . For alkali–metal atoms in the ground state, the tensor shift can vanish once light detuning δ exceeds the hyperfine splitting Δ_{HF} . The ground state is $J = 1/2$, which induces the tensor shift coefficient $\alpha^{(2)} = 0$ [44,46,47]. In this work, we consider a far detuning of $\delta \gg \Delta_{\text{HF}}$, so that the ac Stark shift includes only two terms of scalar $\alpha^{(0)}$ and vector shifts $\alpha^{(1)}$.

For a linearly polarized light beam ($\xi = 0$), the vector shift vanishes, but the scalar shift remains. For circular polarization light, left and right circular polarizations can change the sign of the vector shift to be positive or negative. Therefore, the different ac Stark shifts of two spin states can be canceled by controlling the ellipticity, or tuning the angle between \hat{e}_k and \hat{e}_B (even changing the strength of the external bias magnetic field when considering high order contribution [42,48,49]), which is an important technique for the atomic clock and qubit for quantum computation.

B. Scalar and Vector Shifts

For the first excited state of alkali–metal atoms, the fine structure induces the spectral lines of the D1 ($5^2S_{1/2} \rightarrow 5^2P_{1/2}$ transition) and D2 ($5^2S_{1/2} \rightarrow 5^2P_{3/2}$ transition) lines. Because the D1 and D2 lines of the first excited state are larger detuned than the excited-state hyperfine splitting, the coefficients of the scalar and vector shifts in Eq. (1) are expressed as [50–53]

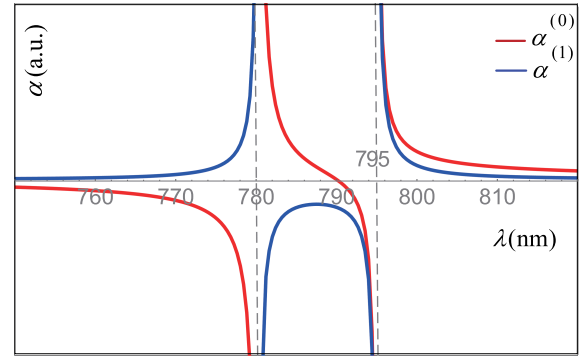


Fig. 1. Coefficients of scalar and vector shifts as a function of wavelength for ^{87}Rb atom in $|F = 2, m_F = 2\rangle$ state. $\alpha^{(0)}$ has a crossed zero point at $\lambda = 790.020$ nm. When the wavelength of light is far red-detuned from D1, $\alpha^{(0)} \gg \alpha^{(1)} \approx 0$.

$$\begin{aligned} \alpha^{(0)}(\omega) &\approx -\frac{\pi c^2 \Gamma_{D2}}{2\omega_0^3} \left(\frac{2}{\delta_{D2}} + \frac{1}{\delta_{D1}} \right), \\ \alpha^{(1)}(\omega) &\approx -\frac{\pi c^2 \Gamma_{D2}}{2\omega_0^3} \left(\frac{1}{\delta_{D2}} - \frac{1}{\delta_{D1}} \right) g_F F, \\ \alpha^{(2)}(\omega) &\approx 0, \end{aligned} \quad (2)$$

where Γ_{D2} is the decay rate of the excited state for the $D2$ line, $\delta_{D1} = \omega - \omega_{D1}$, and $\delta_{D2} = \omega - \omega_{D2}$. g_F is the gyromagnetic ratio

$$\begin{aligned} g_F &= g_J \left[\frac{F(F+1) + J(J+1) - I(I+1)}{2F(F+1)} \right], \\ g_J &= 1 + \frac{J(J+1) + S(S+1) - L(L+1)}{2J(J+1)}, \end{aligned} \quad (3)$$

where S is the spin angular momentum, L is the orbital angular momentum, J is the total electronic angular momentum, and I is the total nuclear angular momentum. For the ground states $5^2S_{1/2}$ of ^{87}Rb atoms, $g_J = 2$, $g_F = 1/2$ for $F = 2$, and $g_F = -1/2$ for $F = 1$. Here, we study ^{87}Rb atoms and present the coefficients of scalar and vector shifts as a function of wavelength in Fig. 1. The resonant wavelengths of the D1 and D2 lines of ^{87}Rb atoms are $\lambda_{D1} = 794.98$ nm and $\lambda_{D2} = 780.24$ nm, respectively. Obviously, $\alpha^{(0)}$ has a crossed zero point at $\lambda = 790.005$ nm, and $\alpha^{(1)}$ is always negative between the D1 and D2 lines. When the wavelength of light is far red-detuned or blue-detuned by an amount larger than the fine structure splitting of the excited states, the vector shift approaches zero. Here, we study the tune-out wavelengths in more general cases of considering the contributions from both scalar and vector shifts. The tune-out wavelengths of the ground hyperfine states are given in Table 1 with $\phi = 0$, $\xi = 0, \pm 1$.

To measure the tune-out wavelengths, we employ a one-dimensional (1D) optical lattice along the external bias magnetic field ($\phi = 0$) with different polarization configurations. Here, the two laser beams have the same intensity with $A = 2\epsilon_0 c |E_1|^2 = 2\epsilon_0 c |E_2|^2$. For case 1, two laser beams with the same linear polarization counterpropagate along the z axis. Because of the parallel polarized beams, it can produce spatial intensity modulation to form a 1D optical lattice:

Table 1. Tune-Out Wavelengths of Ground States with $\phi = 0$ in $5^2S_{1/2} - 5^2P_{1/2, 3/2}$ States of ^{87}Rb

Polarization	$ F, m_F\rangle$	λ_{zero} (nm)			
		Calc. Using Eq. (3)	Calc. in Ref. [17]	Other Calc.	Expt.
$\xi = 0$	$ 2, 2\rangle$	790.005	790.04		790.01850(9) [26]
	$ 2, 1\rangle$	790.005	790.04	790.032439(35) [25]	
	$ 2, 0\rangle$	790.005	790.03	790.034(7) [20]	790.032388(32) [25]
	$ 2, -1\rangle$	790.005	790.04	790.032602(193) [54]	
	$ 2, -2\rangle$	790.005	790.04		
	$ 1, 1\rangle$	790.005	790.04		789.85(1) [55]
	$ 1, 0\rangle$	790.005	790.04	790.018187(193) [54]	790.018(2) [56], 790.020(25) ^a
	$ 1, -1\rangle$	790.005	790.04		790.01858(23) [26]
	$\xi = 1$	$ 2, 2\rangle$	None	None	
$ 2, 1\rangle$		792.484	792.52		
$ 2, 0\rangle$		790.005	790.06		
$ 2, -1\rangle$		787.541	787.59		
$ 2, -2\rangle$		785.093	785.14		
$ 1, 1\rangle$		787.541	787.59		787.590(31) ^a
$ 1, 0\rangle$		790.005	790.06		790.020(25) ^a
$ 1, -1\rangle$		792.484	792.53		
$\xi = -1$		$ 2, 2\rangle$	785.093	785.14	785.11516 [57]
	$ 2, 1\rangle$	787.541	787.59		
	$ 2, 0\rangle$	790.005	790.06		
	$ 2, -1\rangle$	792.484	792.52		
	$ 2, -2\rangle$	None	None	None [57]	
	$ 1, 1\rangle$	792.484	792.53		≈ 792.4 [26], 792.462(22) ^a
	$ 1, 0\rangle$	790.005	790.06		790.020(25) ^a
	$ 1, -1\rangle$	787.541	787.59		≈ 787.620 [26]

^aOur experimental measurements.

$$\Delta U_{L1}(F, m_F; \omega) = -4A\alpha^{(0)} \cos^2 kz. \quad (4)$$

The optical lattice potential for this case originates only from the scalar shift. Therefore it can be used for measuring the tune-out wavelength for the scalar shift. For case 2, two counterpropagating laser beams have linear orthogonal polarization (lin \perp lin polarization configuration). The orthogonally polarized beams cannot produce spatial intensity modulation. In contrast, they can produce the ellipticity modulation of polarization in space. This optical lattice potential is called Sisyphus optical potential, which has been used for Sisyphus cooling [58]. The periodic potential is given by

$$\Delta U_{L2}(F, m_F; \omega) = -2A \left[\alpha^{(0)} + \alpha^{(1)} \xi \frac{m_F}{F} \sin(2kz) \right]. \quad (5)$$

This periodic potential comes only from the vector shift and the scalar term, which gives a uniform energy shift. For case 3, two laser beams with the same circular polarization counterpropagate along the z axis, which can also produce spatial intensity modulation to form a 1D optical lattice:

$$\Delta U_{L3}(F, m_F; \omega) = -4A \cos^2 kz \left[\alpha^{(0)} + \alpha^{(1)} \xi \frac{m_F}{F} \right]. \quad (6)$$

The optical lattice potential for this case includes scalar and vector shifts simultaneously. Therefore, we can study tune-out wavelengths in the presence of contributions of both scalar and vector shifts in this case. For case 4, like case 2, the scalar shift is a constant related only to the constant intensity of two orthogonally polarized counterpropagating laser beams. But

the difference in the former is that the vector shift becomes zero since it produces only rotation of linear polarization in space. Hence it cannot produce any spatial modulation to form a 1D lattice:

$$\Delta U_{L4}(F, m_F; \omega) = -2A\alpha^{(0)}. \quad (7)$$

Here, for a 1D optical lattice along the external bias magnetic field ($|\cos \phi| = 1$), it is convenient to define left and right elliptical polarizations in terms of the magnetic field quantization axis.

3. EXPERIMENT

A schematic of experimental setup is shown in Fig. 2(a). Ultracold ^{87}Rb atoms in the $|F=2, m_F=2\rangle$ hyperfine state are loaded into a crossed optical dipole trap [59]. Forced evaporation in the optical trap is used to create BEC with up to 5×10^5 atoms. To obtain the atoms in different single spin states, BEC is transferred from $|F=2, m_F=2\rangle$ to $|F=1, m_F=1\rangle$ via a rapid adiabatic passage induced by a microwave frequency field with duration of 10 ms at 3.9 G of the bias magnetic field, where the frequency of the center is 6.842935 GHz, and the width is 0.25 MHz. Then the atoms in $|F=1, m_F=1\rangle$ can further be transferred into the $|F=1, m_F=0\rangle$ state using rapid adiabatic passage induced by a radio frequency (rf) field at 28 G of the bias magnetic field. The lattice beam is derived from a single frequency Ti:sapphire laser with a broad tuning range of the frequency. An acousto-optical

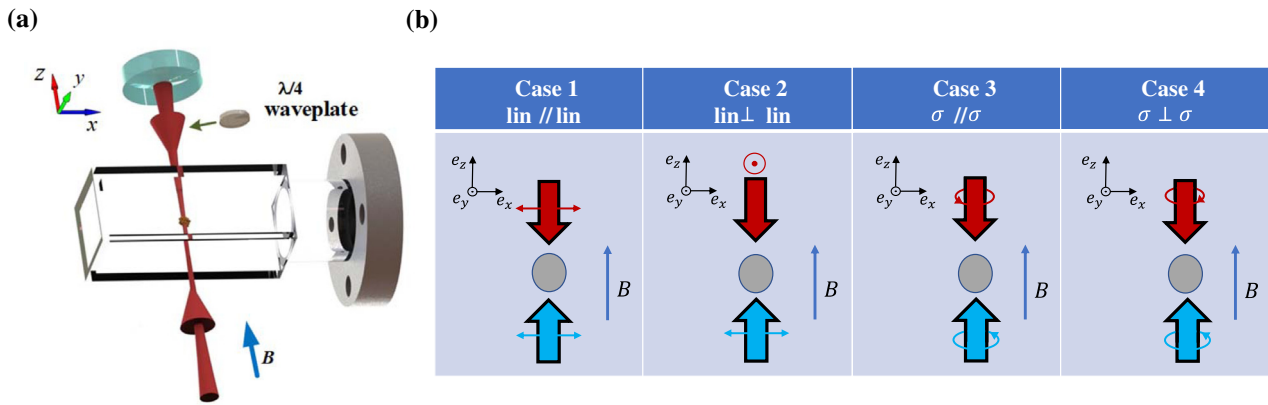


Fig. 2. Schematic of experimental setup and three cases for different polarization configurations. (a) A 1D optical lattice is formed by two counter-propagating laser fields. The external magnetic field is aligned along the z axis. (b) Case 1: counterpropagating lasers have linear parallel polarization. Case 2: counterpropagating lasers have linear orthogonal polarization. Case 3 and Case 4: counterpropagating lasers have circular parallel or orthogonal polarization.

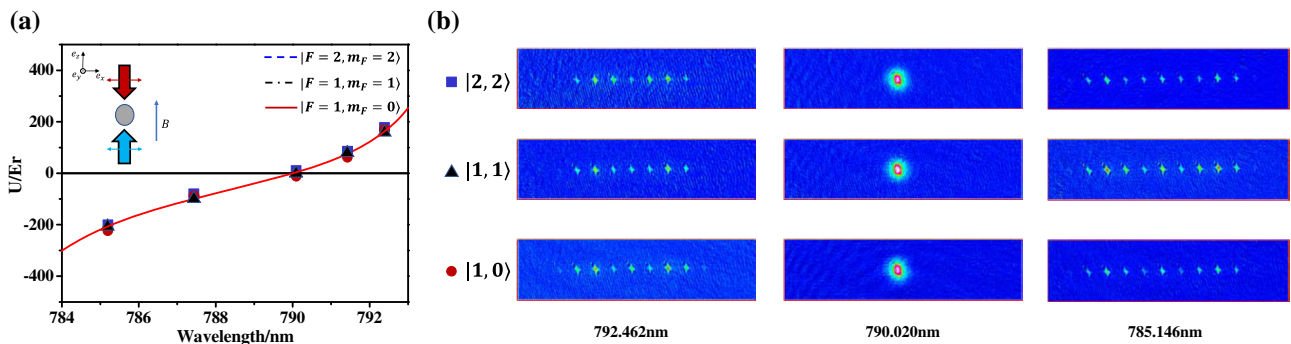


Fig. 3. 1D optical lattice with linear parallel polarization. (a) Measured data (squares, triangles, and circles) and theoretical fit (three types of lines overlapped together) of the lattice potential depth as a function of laser wavelength for the three hyperfine states: $|F = 2, m_F = 2\rangle$, $|F = 1, m_F = 1\rangle$, and $|F = 1, m_F = 0\rangle$. It shows that this periodic potential is a spin-independent lattice. Each point is the average of at least three measurements. (b) Atomic density distribution in the TOF absorption images at different wavelengths of the lattice laser.

modulator is used to control the intensity of the lattice beam. The lattice beam passes through the polarizing beam splitter to generate perfect polarization. The polarization extinction ratio of the polarizing beam splitter can reach 500:1. Therefore, the linear polarization purity of the lattice beam is about 0.2%. Furthermore, the circular polarization purity of the lattice beam can reach about 0.5%. A lattice beam propagates with the z axis and converges on BEC with a waist of $100 \mu\text{m}$ by a lens ($f = 300 \text{ mm}$). Then the beam is reflected by a concave mirror (curvature radius $r = 300 \text{ mm}$) and refocused on BEC with almost the same waist size. The advantage of this configuration is that it can reduce phase jitter significantly. Here, we employ Kapitza–Dirac (or Raman–Nath) scattering to measure the ac Stark shift. Kapitza–Dirac scattering is used to diffract BEC into a number of momentum states by a standing light wave, in which the interaction is sufficiently short and strong [60]. In this process, BEC is kept in a crossed optical dipole trap, and the lattice potential imprints a phase modulation on a matter wave in position space. Then the phase modulation on the matter wave is measured in momentum space via a time-of-flight (TOF) absorption image. It is obvious that higher momentum orders $\pm 2N\hbar k$ appear in the atomic density distribution of the TOF absorption image, which depends on the potential depth and

interaction time. Here, we apply a 1D optical lattice short pulse for $4 \mu\text{s}$ with a power of 80 mW on BEC, then immediately turn off the optical trap, letting the atoms ballistically expand in 12 ms and take the absorption images. We obtain the lattice depth from absorption images by applying the lattice at a fixed laser power for different intervals of time and by observing the interval at which the $n = 0$ order atoms in the lattice vanish [31–35]. We define the recoil momentum $\hbar k = 2\pi\hbar/\lambda$ and recoil energy $E_r = (\hbar k)^2/2m = h \times 3.67 \text{ kHz}$ as the natural momentum and energy units, where m is the mass of the ^{87}Rb atom, and λ is the wavelength of the lattice laser.

For case 1, a 1D optical lattice with linear parallel polarization produces spatial intensity modulation, which comes only from the scalar shift. Thus it is a spin-independent optical lattice, and the potential depth as a function of the lattice wavelength are plotted in Fig. 3(a). Here, the positive and negative periodic potentials correspond to blue and red detuned lattice lasers. The higher momentum orders $\pm 2N\hbar k$ are observed in the atomic density distribution of the TOF absorption images as shown in Fig. 3(b), which depends on the potential depth. We measure the tune-out wavelengths by changing the lattice wavelength and find its location at $\sim 790.020 \text{ nm}$ for all spin states, which is in good agreement with previous works [25,26].

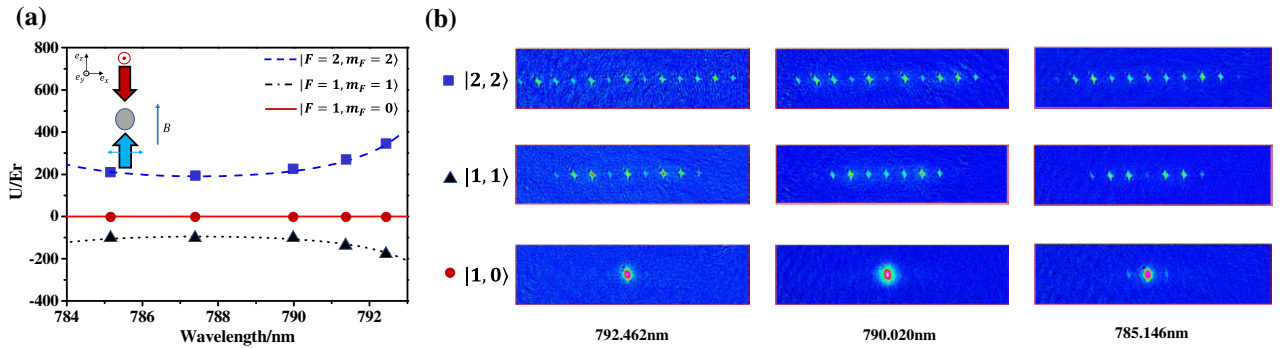


Fig. 4. 1D optical lattice with linear orthogonal polarization. (a) Measured data (squares, triangles, and circles) and theoretical fit (dashed, solid, and dotted lines) of the lattice potential depth as a function of laser wavelength for the three hyperfine states: $|F=2, m_F=2\rangle$, $|F=1, m_F=1\rangle$, and $|F=1, m_F=0\rangle$. This periodic potential is a spin-dependent lattice, which depends only on the vector shift. (b) Atomic density distribution in TOF absorption images at different wavelengths of the lattice laser. There is no lattice potential for the $|F=1, m_F=0\rangle$ state ($\Delta m_F=0$), while the $|m_F=\pm 2\rangle$ and $|m_F=\pm 1\rangle$ states ($\Delta m_F \neq 0$) always experience the lattice potential when adjusting the lattice wavelength.

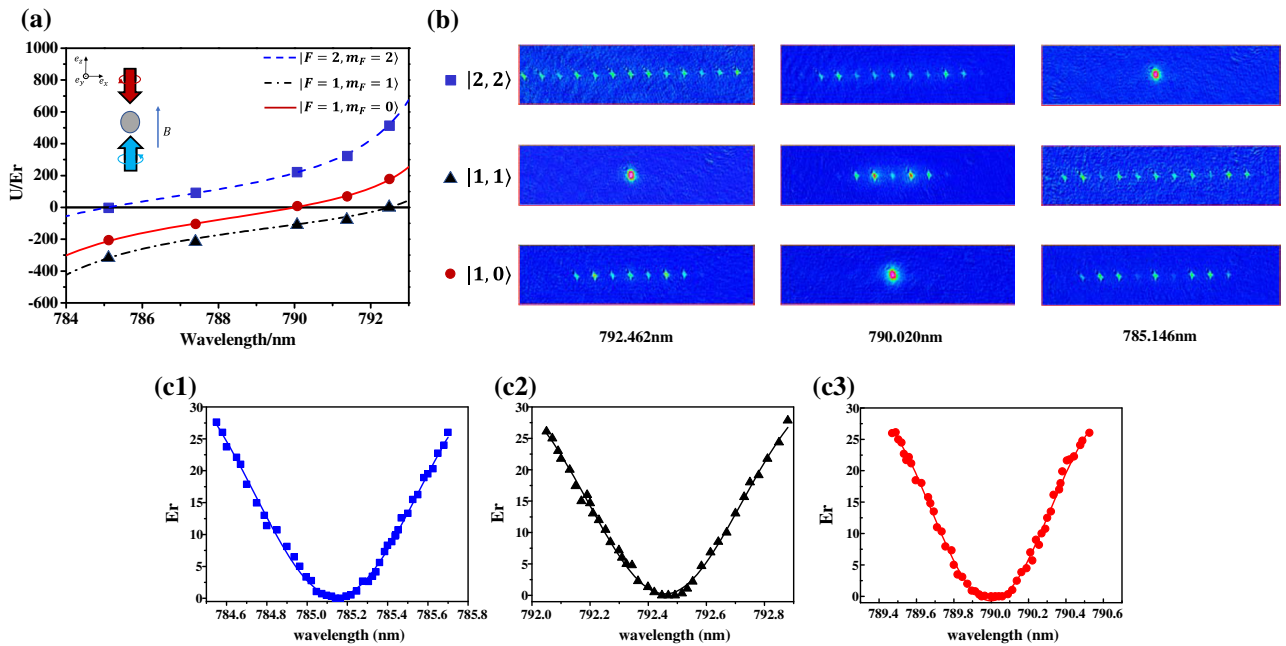


Fig. 5. 1D optical lattice with circular parallel polarization. (a) Measured data (squares, triangles, and circles) and theoretical fit (dashed, solid, and dotted lines) of the lattice potential depth as a function of laser wavelength for the three hyperfine states: $|F=2, m_F=2\rangle$, $|F=1, m_F=1\rangle$, and $|F=1, m_F=0\rangle$. This periodic potential is a spin-dependent lattice, which depends on scalar and vector shifts. Tune-out wavelengths are 792.462(22) nm, 790.020(25) nm, and 785.146(12) nm for $|F=1, m_F=1\rangle$, $|F=1, m_F=0\rangle$, and $|F=2, m_F=2\rangle$, respectively. (b) Atomic density distribution in TOF absorption images at different wavelengths of the lattice laser. (c1)–(c3) Detailed measurements of lattice potentials for $|F=1, m_F=1\rangle$, $|F=1, m_F=0\rangle$, and $|F=2, m_F=2\rangle$ near the tune-out wavelengths, respectively.

For case 2, a laser beam with linear polarization passes through a quarter-wave plate and is reflected by a concave mirror, which produces the linear orthogonal polarization configuration. We plot the potential depth versus different wavelengths as shown in Fig. 4(a). This periodic potential is a spin-dependent lattice, which comes only from the contribution of the vector shift. Therefore, there is no lattice potential for the $|F=1, m_F=0\rangle$ state ($\Delta m_F=0$) for any wavelength as shown in Fig. 4(b). The $|m_F=\pm 2\rangle$ and $|m_F=\pm 1\rangle$ states ($\Delta m_F \neq 0$) always experience the lattice potential when adjusting the lattice wavelength.

For case 3, a 1D optical lattice with circular parallel polarization produces spatial intensity modulation, which includes the contribution of scalar and vector shifts simultaneously. The potential depths of $|F=1, m_F=1\rangle$, $|F=1, m_F=0\rangle$, and $|F=2, m_F=2\rangle$ are given in Figs. 5(a) and 5(b). The tune-out wavelengths are generated by balancing scalar and vector shifts, which are 792.462(22) nm, 790.020(25) nm, and 785.146(12) nm for $|F=1, m_F=1\rangle$, $|F=1, m_F=0\rangle$, and $|F=2, m_F=2\rangle$, respectively as shown in Fig. 5(c). Note that the tune-out wavelengths in this case are sensitive to the ellipticity of lattice polarization, the alignment between the direction of the 1D optical lattice and the external bias magnetic

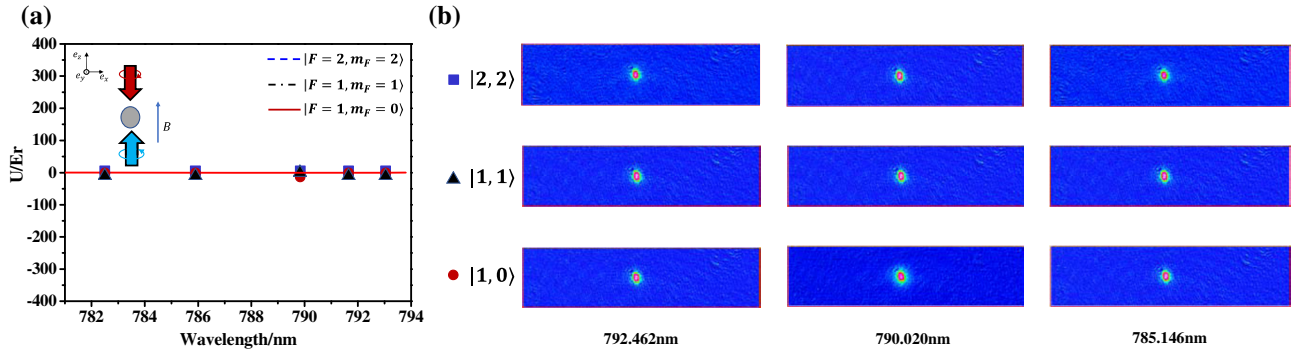


Fig. 6. 1D optical lattice with circular orthogonal polarization. (a) Measured data (squares, triangles, and circles) and theoretical fit (three types of lines overlapped together) of the lattice potential depth as a function of laser wavelength for the three hyperfine states: $|F = 2, m_F = 2\rangle$, $|F = 1, m_F = 1\rangle$, and $|F = 1, m_F = 0\rangle$. There is no obvious periodic potential in this spin-dependent lattice, because the scalar and vector do not produce spatial light intensity modulation. (b) Atomic density distribution of time-of-flight absorption images. There is no lattice potential for any state for any wavelength.

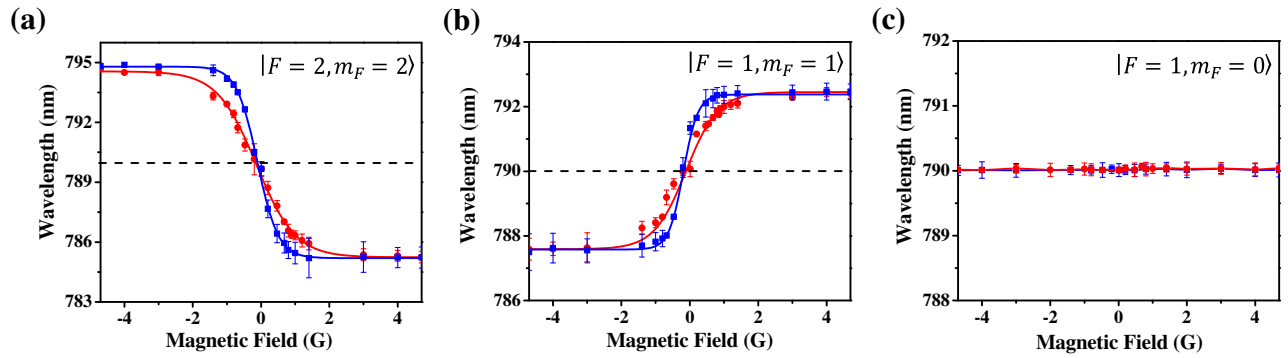


Fig. 7. Tune-out wavelengths as a function of the amplitude of the external magnetic field for Case 3. (a)–(c) $|F = 2, m_F = 2\rangle$, $|F = 1, m_F = 1\rangle$, and $|F = 1, m_F = 0\rangle$, respectively. Blue (square sign) and red (circular sign) curves correspond to the residual magnetic field in the (x, y, z) directions suppressed from $(0.4 \text{ G}, 0.46 \text{ G}, 0.38 \text{ G})$ to $(0.25 \text{ G}, 0.28 \text{ G}, 0.2 \text{ G})$, respectively.

field. This case provides us more controlled ways to generate the different kinds of spin-dependent optical lattice. There is an interesting phenomenon that two neighboring spin states have opposite lattice potential (blue and red detunings) by choosing the appropriate wavelength; for example, $|F = 1, m_F = 1\rangle$ and $|F = 1, m_F = 0\rangle$ states have opposite lattice potential at the wavelength of 791.24 nm.

For case 4, two counterpropagating laser beams with orthogonal circular polarization cannot generate any spatial modulation on BEC. The potential depths for $|F = 1, m_F = 1\rangle$, $|F = 1, m_F = 0\rangle$, and $|F = 2, m_F = 2\rangle$ are given in Figs. 6(a) and 6(b), showing no effective potential (no density modulation) for these states.

Furthermore, we study the dependence of tune-out wavelengths on the strength of the external bias magnetic field in more detail. The intersection angle ϕ between \hat{e}_k and \hat{e}_B is expressed as

$$\cos(\phi) = \frac{B_{\text{Bi}}^z + B_{\text{Re}}^z}{\sqrt{(B_{\text{Re}}^x)^2 + (B_{\text{Re}}^y)^2 + (B_{\text{Bi}}^z + B_{\text{Re}}^z)^2}}, \quad (8)$$

where B_{Bi} is the external bias magnetic field, B_{Re} is the residual magnetic field (such as Earth's magnetic field). We measure

tune-out wavelengths as a function of the strength of the external bias magnetic field as shown in Fig. 7. By changing the bias magnetic field to a small value, the direction of the total magnetic field and the intersection angle ϕ can be changed. Therefore, the tune-out wavelengths change when the strength of the bias magnetic field is near the residual magnetic field value. The strength of the external bias magnetic field in one direction is gradually decreased to zero and then increased in the opposite direction. We find that the tune-out wavelengths for $\xi = 1$ jump to $\xi = -1$ due to inversion of the external bias magnetic field direction for the spin $|F = 1, m_F = 1\rangle$ and $|F = 2, m_F = 2\rangle$ states as shown in Figs. 7(a) and 7(b). The slope is sensitive to the strength of the residual magnetic field in the perpendicular direction of the z axis. Here, three pairs of Helmholtz coils are employed to compensate for the background magnetic field. When the residual magnetic field in (x, y, z) directions are suppressed from $(0.4 \text{ G}, 0.46 \text{ G}, 0.38 \text{ G})$ to $(0.25 \text{ G}, 0.28 \text{ G}, 0.2 \text{ G})$, measured by a triaxial flux-gate magnetometer, the slope is changed from -4.054 nm/G to -6.584 nm/G for $|F = 1, m_F = 1\rangle$ and 8.108 nm/G to 13.168 nm/G for $|F = 2, m_F = 2\rangle$ as shown in Figs. 7(a) and 7(b), respectively. Therefore, this method can be utilized to calibrate and measure the residual magnetic field.

4. CONCLUSION

In conclusion, we present an experiment to measure the ac Stark shift around the tune-out wavelengths of ^{87}Rb BEC in three different hyperfine ground states, $|F = 1, m_F = 1\rangle$, $|F = 1, m_F = 0\rangle$ and $|F = 2, m_F = 2\rangle$, between D1 and D2 lines. Four different polarization configurations of a 1D optical lattice, which are originated from the scalar shift, vector shift, and both scalar and vector shifts by manipulating lattice polarizations, are investigated. The Kapitza–Dirac scattering technique is employed to probe the ac Stark shift of atoms in an optical lattice, and the characteristics of a spin-dependent optical lattice are presented by scanning the lattice wavelength. We present tune-out wavelengths in more general cases of considering the contributions of both scalar and vector shifts. We further study the dependence of tune-out wavelengths on the strength of the external bias magnetic field in more detail. Our work provides a clear interpretation of spin-dependent optical lattices and can be used for realization of a two-species system, or the same atoms (Rb) with different spin states, in which one of them moves freely while the others are trapped to different degrees of optical lattice potential. This system can be a test-bed for observing or simulating phenomena such as entropy cooling [20,52,55,56,61], Kondo effect [62,63], etc., and even have application in Sr optical lattice clocks [64].

Funding. National Key Research and Development Program of China (2016YFA0301602, 2018YFA0307601); National Natural Science Foundation of China (11804203, 11974224, 12004229, 12022406, 12034011, 92065108); Shanxi Key Subjects Construction (1331); The Program of Youth Sanjin Scholar.

Disclosures. The author declares no conflicts of interest.

Data Availability. Data underlying the results presented in this paper are not publicly available at this time but may be obtained from the authors upon reasonable request.

REFERENCES

- I. Bloch, J. Dalibard, and W. Zwerger, “Many-body physics with ultracold gases,” *Rev. Mod. Phys.* **80**, 885–964 (2008).
- M. Aidelsburger, M. Atala, M. Lohse, J. T. Barreiro, B. Paredes, and I. Bloch, “Realization of the Hofstadter Hamiltonian with ultracold atoms in optical lattices,” *Phys. Rev. Lett.* **111**, 185301 (2013).
- H. Miyake, G. A. Siviloglou, C. J. Kennedy, W. C. Burton, and W. Ketterle, “Realizing the Harper Hamiltonian with laser-assisted tunneling in optical lattices,” *Phys. Rev. Lett.* **111**, 185302 (2013).
- C. S. Chiu, G. Ji, A. Mazurenko, D. Greif, and M. Greiner, “Quantum state engineering of a Hubbard system with ultracold fermions,” *Phys. Rev. Lett.* **120**, 243201 (2018).
- U. Schnorrberger, J. D. Thompson, S. Trotzky, R. Pugatch, N. Davidson, S. Kuhr, and I. Bloch, “Electromagnetically induced transparency and light storage in an atomic Mott insulator,” *Phys. Rev. Lett.* **103**, 033003 (2009).
- M. J. Martin, M. Bishop, M. D. Swallows, X. Zhang, C. Benko, J. von Stecher, A. V. Gorshkov, A. M. Rey, and J. Ye, “A quantum many-body spin system in an optical lattice clock,” *Science* **341**, 632–636 (2013).
- O. Mandel, M. Greiner, A. Widera, T. Rom, T. W. Hänsch, and I. Bloch, “Coherent transport of neutral atoms in spin-dependent optical lattice potentials,” *Phys. Rev. Lett.* **91**, 010407 (2003).
- L. M. Duan, E. Demler, and M. D. Lukin, “Controlling spin exchange interactions of ultracold atoms in optical lattices,” *Phys. Rev. Lett.* **91**, 090402 (2003).
- P. Soltan-Panahi, J. Struck, P. Hauke, A. Bick, W. Plenkers, G. Meineke, C. Becker, P. Windpassinger, M. Lewenstein, and K. Sengstock, “Multi-component quantum gases in spin-dependent hexagonal lattices,” *Nat. Phys.* **7**, 434–440 (2011).
- B. Yang, H. Dai, H. Sun, A. Reingruber, Z. Yuan, and J. Pan, “Spin-dependent optical superlattice,” *Phys. Rev. A* **96**, 011602 (2017).
- Y. Ke, J. Huang, M. Zhuang, B. Lu, and C. Lee, “Compact gravimeter with an ensemble of ultracold atoms in spin-dependent optical lattices,” *Phys. Rev. A* **98**, 053826 (2018).
- E. A. Ostrovskaya and Y. S. Kivshar, “Localization of two-component Bose-Einstein condensates in optical lattices,” *Phys. Rev. Lett.* **92**, 180405 (2004).
- Q. Ye, X. Qin, Y. Li, H. Zhong, Y. S. Kivshar, and C. Lee, “Band-gap structure and chiral discrete solitons in optical lattices with artificial gauge fields,” *Ann. Phys.* **388**, 173–185 (2018).
- F. Grusdt, T. Li, I. Bloch, and E. Demler, “Tunable spin-orbit coupling for ultracold atoms in two-dimensional optical lattices,” *Phys. Rev. A* **95**, 063617 (2017).
- L. Krinner, M. Stewart, A. Pazmino, J. Kwon, and D. Schneble, “Spontaneous emission of matter waves from a tunable open quantum system,” *Nature* **559**, 589–592 (2018).
- A. González-Tudela and J. I. Cirac, “Cold atoms in twisted-bilayer optical potentials,” *Phys. Rev. A* **100**, 053604 (2019).
- L. J. LeBlanc and J. H. Thywissen, “Species-specific optical lattices,” *Phys. Rev. A* **75**, 053612 (2007).
- L. W. Clark, L. Ha, C. Xu, and C. Chin, “Quantum dynamics with spatiotemporal control of interactions in a stable Bose-Einstein condensate,” *Phys. Rev. Lett.* **115**, 155301 (2015).
- R. Trubko, J. Greenberg, M. T. S. Germaine, M. D. Gregoire, W. F. Holmgren, I. Hromada, and A. D. Cronin, “Atom interferometer gyroscope with spin-dependent phase shifts induced by light near a tune-out wavelength,” *Phys. Rev. Lett.* **114**, 140404 (2015).
- B. Arora, M. S. Safronova, and C. W. Clark, “Tune-out wavelengths of alkali-metal atoms and their applications,” *Phys. Rev. A* **84**, 043401 (2011).
- J. Jiang, L. Tang, and J. Mitroy, “Tune-out wavelengths for potassium,” *Phys. Rev. A* **87**, 032518 (2013).
- Y. Cheng, J. Jiang, and J. Mitroy, “Tune-out wavelengths for the alkaline-earth-metal atoms,” *Phys. Rev. A* **88**, 022511 (2013).
- W. F. Holmgren, R. Trubko, I. Hromada, and A. D. Cronin, “Measurement of a wavelength of light for which the energy shift for an atom vanishes,” *Phys. Rev. Lett.* **109**, 243004 (2012).
- B. M. Henson, R. I. Khakimov, R. G. Dall, K. G. H. Baldwin, L. Tang, and A. G. Truscott, “Precision measurement for metastable helium atoms of the 413 nm tune-out wavelength at which the atomic polarizability vanishes,” *Phys. Rev. Lett.* **115**, 043004 (2015).
- R. H. Leonard, A. J. Fallon, C. A. Sackett, and M. S. Safronova, “High-precision measurements of the ^{87}Rb D-line tune-out wavelength,” *Phys. Rev. A* **92**, 052501 (2015).
- F. Schmidt, D. Mayer, M. Hohmann, T. Lausch, F. Kindermann, and A. Widera, “Precision measurement of the ^{87}Rb tune-out wavelength in the hyperfine ground state $F = 1$ at 790 nm,” *Phys. Rev. A* **93**, 022507 (2016).
- F. Adam and S. Charles, “Obtaining atomic matrix elements from vector tune-out wavelengths using atom interferometry,” *Atoms* **4**, 12 (2016).
- R. Trubko, M. D. Gregoire, W. F. Holmgren, and A. D. Cronin, “Potassium tune-out-wavelength measurement using atom interferometry and a multipass optical cavity,” *Phys. Rev. A* **95**, 052507 (2017).
- E. Copenhaver, K. Cassella, R. Berghaus, and H. Müller, “Measurement of a ^7Li tune-out wavelength by phase-patterned atom interferometry,” *Phys. Rev. A* **100**, 063603 (2019).
- B. Décamps, J. Vigué, A. Gauguier, and M. Büchner, “Measurement of the 671 nm tune-out wavelength of ^7Li by atom interferometry,” *Phys. Rev. A* **101**, 033614 (2020).
- Y. B. Ovchinnikov, J. H. Müller, M. R. Doery, E. J. D. Vredenburg, K. Helmerson, S. L. Rolston, and W. D. Phillips, “Diffraction of a released Bose-Einstein condensate by a pulsed standing light wave,” *Phys. Rev. Lett.* **83**, 284–287 (1999).
- S. B. Cahn, A. Kumarakrishnan, U. Shim, T. Sleator, P. R. Berman, and B. Dubetsky, “Time-domain de Broglie wave interferometry,” *Phys. Rev. Lett.* **79**, 784–787 (1997).

33. J. H. Denschlag, J. Simsarian, H. Häffner, C. McKenzie, A. Browaeys, D. Cho, K. Helmerson, S. Rolston, and W. D. Phillips, "A Bose-Einstein condensate in an optical lattice," *J. Phys. B* **35**, 3095 (2002).
34. B. T. Beswick, I. G. Hughes, and S. A. Gardiner, "Lattice-depth measurement using multipulse atom diffraction in and beyond the weakly diffracting limit," *Phys. Rev. A* **99**, 013614 (2019).
35. H. Chen, D. Xiong, P. Wang, and J. Zhang, "Pulse loading ^{87}Rb Bose-Einstein condensation in optical lattice: the Kapitza-Dirac scattering and temporal matter-wave-dispersion Talbot effect," *Chin. Opt. Lett.* **8**, 348–350 (2010).
36. K. Viebahn, M. Sbroscia, E. Carter, J. C. Yu, and U. Schneider, "Matter-wave diffraction from a quasicrystalline optical lattice," *Phys. Rev. Lett.* **122**, 110404 (2019).
37. K. Wen, Z. Meng, P. Wang, L. Wang, L. Chen, L. Huang, L. Zhou, X. Cui, and J. Zhang, "Observation of sub-wavelength phase structure of matter wave with two-dimensional optical lattice by Kapitza-Dirac diffraction," *Sci. Rep.* **10**, 5870 (2020).
38. J. Stenger, S. Inouye, A. P. Chikkatur, D. M. Stamper-Kurn, D. E. Pritchard, and W. Ketterle, "Bragg spectroscopy of a Bose-Einstein condensate," *Phys. Rev. Lett.* **82**, 4569–4573 (1999).
39. S. Gupta, K. Dieckmann, Z. Hadzibabic, and D. E. Pritchard, "Contrast interferometry using Bose-Einstein condensates to measure h/m and α ," *Phys. Rev. Lett.* **89**, 140401 (2002).
40. G. K. Campbell, A. E. Leanhardt, J. Mun, M. Boyd, E. W. Streed, W. Ketterle, and D. E. Pritchard, "Photon recoil momentum in dispersive media," *Phys. Rev. Lett.* **94**, 170403 (2005).
41. K. Beloy, "Theory of the AC Stark effect on the atomic hyperfine structure and applications to microwave atomic clocks," Ph.D. thesis (University of Nevada, 2009).
42. N. Lundblad, M. Schlosser, and J. V. Porto, "Experimental observation of magic-wavelength behavior of ^{87}Rb atoms in an optical lattice," *Phys. Rev. A* **81**, 031611 (2010).
43. F. Le Kien, P. Schneeweiss, and A. Rauschenbeutel, "Dynamical polarizability of atoms in arbitrary light fields: general theory and application to cesium," *Eur. Phys. J. D* **67**, 92 (2013).
44. J. H. Becher, S. Baier, K. Aikawa, M. Lepers, J. F. Wyart, O. Dulieu, and F. Ferlaino, "Anisotropic polarizability of erbium atoms," *Phys. Rev. A* **97**, 012509 (2018).
45. V. V. Tsyganok, D. A. Pershin, E. T. Davletov, V. A. Khlebnikov, and A. V. Akimov, "Scalar, tensor, and vector polarizability of TM atoms in a 532 nm dipole trap," *Phys. Rev. A* **100**, 042502 (2019).
46. D. A. Steck, *Quantum and Atom Optics* (2007).
47. P. Rosenbusch, S. Ghezali, V. A. Dzuba, V. V. Flambaum, K. Beloy, and A. Derevianko, "AC Stark shift of the Cs microwave atomic clock transitions," *Phys. Rev. A* **79**, 013404 (2009).
48. A. Derevianko, "Theory of magic optical traps for Zeeman-insensitive clock transitions in alkali-metal atoms," *Phys. Rev. A* **81**, 051606 (2010).
49. J. Yang, X. He, R. Guo, P. Xu, K. Wang, C. Sheng, M. Liu, J. Wang, A. Derevianko, and M. Zhan, "Coherence preservation of a single neutral atom qubit transferred between magic-intensity optical traps," *Phys. Rev. Lett.* **117**, 123201 (2016).
50. K. L. Corwin, S. J. M. Kuppens, D. Cho, and C. E. Wieman, "Spin-polarized atoms in a circularly polarized optical dipole trap," *Phys. Rev. Lett.* **83**, 1311–1314 (1999).
51. C. Y. Park, H. Noh, C. M. Lee, and D. Cho, "Measurement of the Zeeman-like AC Stark shift," *Phys. Rev. A* **63**, 032512 (2001).
52. D. McKay and B. Demarco, "Thermometry with spin-dependent lattices," *New J. Phys.* **12**, 055013 (2010).
53. M. Cao, L. Han, Y. Qi, S. Zhang, G. Hong, and F. Li, "Calculation of the spin-dependent optical lattice in rubidium Bose-Einstein condensation," *Chin. Rev. Lett.* **29**, 034201 (2012).
54. X. Wang, J. Jiang, L. Xie, D. Zhang, and C. Dong, "Polarizabilities and tune-out wavelengths of the hyperfine ground states of $^{87,85}\text{Rb}$," *Phys. Rev. A* **94**, 052510 (2016).
55. J. Catani, G. Barontini, G. Lamporesi, F. Rabatti, G. Thalhammer, F. Minardi, S. Stringari, and M. Inguscio, "Entropy exchange in a mixture of ultracold atoms," *Phys. Rev. Lett.* **103**, 140401 (2009).
56. G. Lamporesi, J. Catani, G. Barontini, Y. Nishida, M. Inguscio, and F. Minardi, "Scattering in mixed dimensions with ultracold gases," *Phys. Rev. Lett.* **104**, 153202 (2010).
57. X. Wang, "Theoretical study of the polarizabilities, tune-out wavelengths, and magic wavelengths of Rb atom," Master's thesis (University of Northwest Normal, 2017).
58. J. Dalibard and C. Cohen-Tannoudji, "Laser cooling below the Doppler limit by polarization gradients: simple theoretical models," *J. Opt. Soc. Am. B* **6**, 2023–2045 (1989).
59. D. Xiong, P. Wang, Z. Fu, S. Chai, and J. Zhang, "Evaporative cooling of ^{87}Rb atoms into Bose-Einstein condensate in an optical dipole trap," *Chin. Opt. Lett.* **8**, 627–629 (2010).
60. P. L. Gould, G. A. Ruff, and D. E. Pritchard, "Diffraction of atoms by light: the near-resonant Kapitza-Dirac effect," *Phys. Rev. Lett.* **56**, 827–830 (1986).
61. R. Bause, M. Li, A. Schindewolf, X. Chen, M. Duda, S. Kotochigova, I. Bloch, and X. Luo, "Tune-out and magic wavelengths for ground-state $^{23}\text{Na}^{40}\text{K}$ molecules," *Phys. Rev. Lett.* **125**, 023201 (2020).
62. R. Zhang, D. Zhang, Y. Cheng, W. Chen, P. Zhang, and H. Zhai, "Kondo effect in alkaline-earth-metal atomic gases with confinement-induced resonances," *Phys. Rev. A* **93**, 043601 (2016).
63. J. Yao, H. Zhai, and R. Zhang, "Efimov-enhanced Kondo effect in alkali-metal and alkaline-earth-metal atomic gas mixtures," *Phys. Rev. A* **99**, 010701 (2019).
64. A. Heinz, A. J. Park, N. S. Šantić, J. Trautmann, S. G. Porsev, M. S. Safronova, I. Bloch, and S. Blatt, "State-dependent optical lattices for the strontium optical qubit," *Phys. Rev. Lett.* **124**, 203201 (2020).